Adaptive Maximum Power Point Tracking Control Algorithm for Wind Energy Conversion Systems

Jakeer Hussain, *Student Member, IEEE*, and Mahesh K. Mishra, *Senior Member, IEEE*

***Abstract*—This paper presents an adaptive maximum power point tracking (MPPT) algorithm for small-scale wind energy conversion systems (WECSs) to harvest more energy from turbulent wind. The proposed algorithm combines the computational behavior of hill climb search, tip speed ratio, and power signal feedback control algorithms for its adaptability over wide range of WECSs and fast tracking of maximum power point. In this paper, the proposed MPPT algorithm is implemented by using buck–boost featured single-ended primary inductor converter to extract maximum power from full range of wind velocity profile. Evaluation of the proposed algorithm is done on a laboratory-scaled dc motor drive-based WECS emulator. TMS320F28335, 32-bit floating point digital signal controller, is used to execute the control schemes of the in-lab experimental setup. Experimental results show that tracking capability of the proposed algorithm under sudden and gradual fluctuating wind conditions is efficient and effective.**

***Index Terms*—Maximum power point tracking, hill climb search algorithm, tip speed ratio algorithm, power signal feedback algorithm, single-ended primary inductor converter (SEPIC) dc-dc converter.**

I. Introduction

INTEREST in renewable energy is increasing as alternative energy source to conventional fossil fuel, because of latter's soaring prices, limited reserve capacity, and environmental concerns. Across the globe, research community is exploring all possibilities for the efficient energy conversion from freely available abundant renewable energy sources. Among the popular renewable energy sources, wind energy is gaining more support due to its less space occupancy and zero-carbon emission during operation. Variable speed wind energy conversion systems (WECSs) can harness more electrical energy than fixed speed WECSs by controlling their speed according to the variations in wind velocity [1], [2]. Maximum power point tracking (MPPT) algorithms are used to extract maximum power from the available wind energy and they are classified into three categories, namely tip speed ratio (TSR) control, power signal feedback (PSF) control and hill climb search (HCS) control [3]. In TSR control method, rotational speed of the wind generator (WG) is regulated in order to maintain the TSR to an optimum value at which power extraction is maximum. Optimal speed for the turbine ω_m^* (rad/s) is calculated by using wind velocity V_w (m/s), turbine rotating speed ω_m (rad/s), and optimal TSR $\lambda_{\rm opt}$ of the system as follows [4]–[6],

$$\omega_m^* = \frac{\lambda_{\rm opt} V_w}{R} \tag{1}$$

where R is rotor radius in meter. Implementation of TSR algorithm requires the knowledge of $\lambda_{\rm opt}$ of the turbine and is system dependent.

In PSF control method, wind turbine operates at optimal operating point by using the prior knowledge of turbine's maximum power curve [7]–[10]. Implementation of this method requires the prior knowledge of maximum power curves which can be obtained through off-line experiments or system simulations. In HCS control method, an arbitrary small perturbation is given to one of the independent variables of the system and next perturbation is decided based on the changes in output power due to preceding perturbation [11], [12]. Drawbacks of this algorithm are, slow tracking response, especially for high inertia systems. Advanced HCS based on-line training algorithms are reported in [13] and [14] to improve the system tracking response of its maximum power point (MPP). In the present work, a simplified algorithm than [14] has been implemented to improve the system tracking response under rapid fluctuating wind velocity conditions.

Microgrid is essentially a collection of distributed energy resources (DERs), potential energy storage devices, and loads connected together to form a relatively small-size distribution network [15]. Small-scale WECSs are main resources for DERs in microgrid systems and are usually installed at congested places with turbulent wind conditions where wind speed and direction vary frequently. Extraction of maximum power with fast tracking control strategy under fluctuating wind conditions is a challenging issue. In small-scale WECSs, power conditioning converter's control is most frequently adapting strategy to extract maximum power since pitch angle control is impractical due to their mechanical structure. In this work buck–boost featured single-ended primary inductor converter (SEPIC) dc–dc converter has been used to extract maximum power from total range of wind velocity profile.

This work assumes that the WECS has effective yaw mechanism to turn the turbine nacelle in the direction of the wind immediately against to the variations in wind flow direction. In this paper, a hybrid nature of MPPT control algorithm which combines the computational behavior of HCS-TSR-PSF algorithms for system independent adaptivity and fast tracking capability of MPP is presented. The proposed MPPT algorithm has been evaluated by using a laboratory scaled DC motor drive based WECS emulator. Experimental results show that the proposed algorithm enables the WECS to harvest more energy by tracking the MPP under turbulent wind conditions.

Manuscript received June 18, 2015; revised September 18, 2015; accepted December 14, 2015. Paper no. TEC-00417-2015.

The authors are with the Department of Electrical Engineering, Indian Institute of Technology Madras, Chennai 600036, India (e-mail: jakeer.s.hussain@gmail.com; mahesh@ee.iitm.ac.in).

Color versions of one or more of the figures in this paper are available online at http://ieeexplore.ieee.org.

Digital Object Identifier 10.1109/TEC.2016.2520460

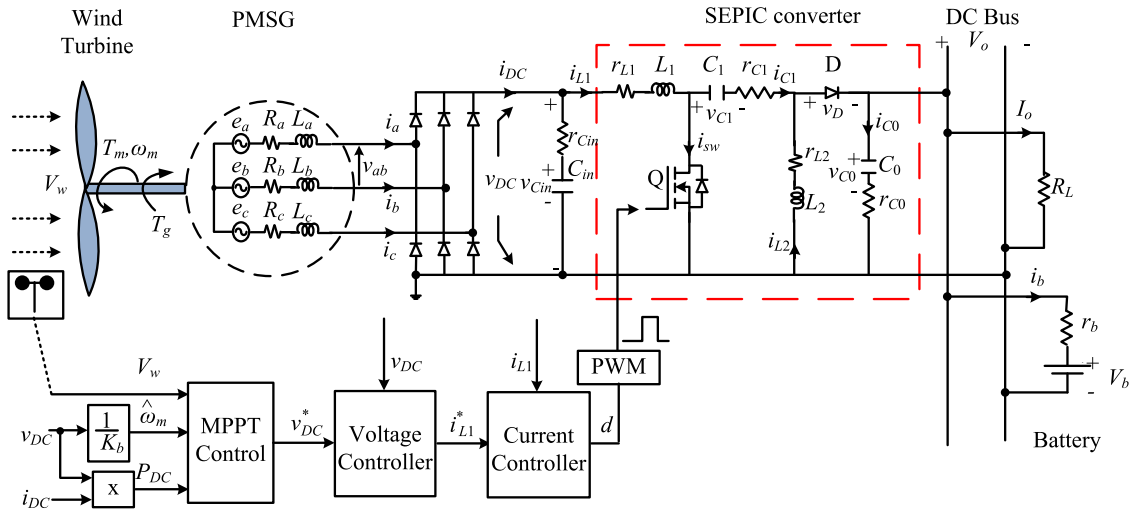

Fig. 1. WECS configuration.

II. System Configuration and Modeling

In the process of developing a laboratory-scaled dc microgrid platform, WECS related system configuration is shown in Fig. 1. In small scale variable speed WECS, direct driven permanent magnet synchronous generator (PMSG) with diode rectifier is the most preferred configuration due to PMSG's high air-gap flux density, and high torque-to-inertia ratio. Its decoupling control performance is much less sensitive to the parameter variations of the generator [16]–[19].

A. Wind Turbine Aerodynamic Model

Mechanical output power P_m extracted from wind by the wind turbine and corresponding torque T_m imparted onto WG can be modeled as [20],

$$P_m = \frac{1}{2}\rho\pi R^2 V_w^3 C_p(\lambda,\beta)$$
$$T_m = \frac{P_m}{\omega_m} \tag{2}$$

where ρ is air density (kg/m^3), C_p is power coefficient which is function of TSR λ and pitch angle β. The coefficient, C_p can be modeled by using rotor blade's aerodynamic design principles [21],

$$C_p(\lambda,\beta) = C_1\left[\frac{C_2}{\lambda_i} - C_3\beta - C_4\right]e^{-C_5/\lambda_i} + C_6\lambda \tag{3}$$

where

$$\frac{1}{\lambda_i} = \frac{1}{\lambda + 0.008\beta} - \frac{0.035}{\beta^2+1}$$

and empirical constants, $C_1 = 0.5176$; $C_2 = 116$; $C_3 = 0.4$; $C_4 = 5$; $C_5 = 21$; $C_6 = 0.0068$.

In this work, DC motor based hardware wind turbine emulator is developed in the laboratory by using (2) and (3).

B. PMSG-Diode Rectifier Model

Induced emf, e_s (V), in stator winding of PMSG, when it is subjected to a constant flux, ϕ (Wb), while rotating with a speed, ω_m (rad/s), is given by

$$e_s = k\,\omega_m = k\,\frac{\omega_e}{P} \tag{4}$$

where k (V·s/rad) is machine induced voltage constant, P is total number of rotor pole pairs and ω_e is electrical angular frequency of PMSG stator induced voltage. In steady state, PMSG's terminal phase voltage, V_s, and output power, P_g, are given by

$$V_s^2 = E_s^2 - (\omega_e L_s I_s)^2$$
$$P_g = 3V_s I_s = 3\sqrt{E_s^2 I_s^2 - (\omega_e L_s)^2 I_s^4} \tag{5}$$

where E_s, I_s and L_s are induced voltage in PMSG's stator winding, stator current and inductance respectively. To derive the basic relations, assuming that both the commutating angle and commutating inductance are negligible, the relation between diode rectifier output voltage, $V_{\rm DC}$ and line voltage at terminals of PMSG, V_t, can be related as [22],

$$V_{\rm DC} = \frac{3\sqrt{2}}{\pi}V_t = \frac{3\sqrt{6}}{\pi}V_s \tag{6}$$

where V_t is RMS value of line-to-line voltage of PMSG. By ignoring the power loss during diode circuit rectification, output power of WECS P_g can be equated to

$$P_g = P_{\rm DC} = 3V_s I_s = V_{\rm DC} I_{\rm DC}. \tag{7}$$

PMSG output power P_g and electromagnetic torque T_g can be expressed as function of diode rectifier output current $I_{\rm DC}$ by using (4)–(7), and are given as

$$P_g = \frac{3\sqrt{6}}{\pi}\omega_g I_{\rm DC}\sqrt{k^2 - \frac{6}{\pi^2}(PL_s)^2 I_{\rm DC}^2}$$
$$T_g = \frac{3\sqrt{6}}{\pi}I_{\rm DC}\sqrt{k^2 - \frac{6}{\pi^2}(PL_s)^2 I_{\rm DC}^2}. \tag{8}$$

Wind turbine rotor speed can be controlled by controlling the generator torque as follows

$$\omega_m = \frac{T_m - T_g}{B_t} \tag{9}$$

where B_t (Nm · s/rad) is turbine rotor friction coefficient. Based on (8) and (9), it can be concluded that by controlling diode rectifier output current, load torque on wind turbine and finally turbine speed can be controlled. This principle is employed to extract maximum power by a given WECS under different wind velocities.

C. Small-Signal Modeling of SEPIC DC–DC Converter

Through off-line experiments on the developed laboratory-scaled wind turbine emulator, it is noticed that operating range of the dc–dc converter's input voltage is 21–135 V. Among the conventional dc–dc converters, boost converter is one of the frequently used dc–dc converters in distributed generation systems, because of its higher efficiency in energy transfer. However, it can able to transfer energy only when its output stage voltage is higher than the input stage voltage. This situation still becomes worse during sudden wind gusts. To extract wind energy from total range of wind velocity profile, a buck–boost featured dc–dc converter is preferable than boost converter as a universal converter. Among the various buck–boost converters, SEPIC dc–dc converter is better choice for WECSs, because it possesses the merits of non inverting polarity, easy-to drive switch [23], and low input-current pulsations, which mitigate the generator's torque pulsations.

Equivalent circuit of the SEPIC dc–dc converter is shown in Fig. 2. Output stage of the SEPIC converter is modeled as a combination of constant voltage source with series internal resistance of the battery. Further, for a given wind velocity and load, the WG and rectifier can be replaced by Thevenin's equivalent voltage, V_{eq} and a series resistor, r_{eq} at input stage of the SEPIC converter [24]. In this work to develop a suitable controller, state-space averaging method [25] is used for small-signal modeling of the SEPIC converter. A small-signal ac model (10) which describes the linear operation of SEPIC based plant, is derived and is given in (11).

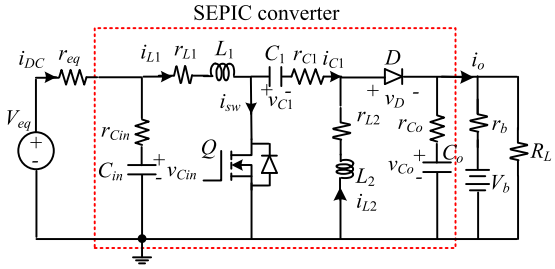

Fig. 2. Equivalent circuit of plant.

$$\dot{\hat{\mathbf{x}}} = \mathbf{A}\hat{\mathbf{x}} + [\mathbf{B} \quad \mathbf{B_D}] \begin{bmatrix} \hat{\mathbf{u}} \\ \hat{\mathrm{d}} \end{bmatrix} \tag{10}$$

$$\begin{bmatrix} \frac{d\hat{v}_{C\text{in}}(t)}{d(t)} \\ \frac{d\hat{i}_{L1}(t)}{d(t)} \\ \frac{d\hat{v}_{C1}(t)}{d(t)} \\ \frac{d\hat{i}_{L2}(t)}{d(t)} \\ \frac{d\hat{v}_{\text{Co}}(t)}{d(t)} \end{bmatrix} = \begin{bmatrix} -\frac{R_{\text{eq}}}{C_{\text{in}} r_{\text{eq}} r_{C\text{in}}} & -\frac{R_{\text{eq}}}{C_{\text{in}} r_{C\text{in}}} & 0 & 0 & 0 \\ \frac{R_{\text{eq}}}{L_1 r_{C\text{in}}} & -\frac{\Delta 1}{L_1} & -\frac{(1-D)}{L_1} & -\frac{R_B\,(1-D)}{L_1} & -\frac{R_B\,(1-D)}{L_1 r_{\text{Co}}} \\ 0 & \frac{(1-D)}{C_1} & 0 & -\frac{D}{C_1} & 0 \\ 0 & -\frac{R_B\,(1-D)}{L_2} & \frac{D}{L_2} & -\frac{\Delta 2}{L_2} & -\frac{R_B\,(1-D)}{L_2 r_{\text{Co}}} \\ 0 & \frac{R_B\,(1-D)}{C_o r_{\text{Co}}} & 0 & \frac{R_B\,(1-D)}{C_o r_{\text{Co}}} & -\frac{R_B}{C_o r_{\text{Co}} r_b} \end{bmatrix} \begin{bmatrix} \hat{v}_{C\text{in}}(t) \\ \hat{i}_{L1}(t) \\ \hat{v}_{C1}(t) \\ \hat{i}_{L2}(t) \end{bmatrix} + \begin{bmatrix} B & B_d \end{bmatrix} \begin{bmatrix} \hat{v}_{\text{eq}} \\ \hat{v}_D \\ \hat{v}_b \\ \hat{d} \end{bmatrix} \tag{11}$$

$$R_{\text{eq}} = \frac{r_{\text{eq}} r_{C\text{in}}}{r_{\text{eq}} + r_{C\text{in}}}, R_B = \frac{r_b r_{\text{Co}}}{r_b + r_{\text{Co}}}, \Delta 1 = (R_B + r_{L1})(1-D) + (R_{\text{eq}} + r_{L1}), \Delta 2 = R_B\,(1-D) + r_{C1} D + r_{L2}$$

$$B = \begin{bmatrix} \frac{R_{\text{eq}}}{C_{\text{in}} r_{\text{eq}} r_{C\text{in}}} & 0 & 0 \\ \frac{R_{\text{eq}}}{L_1 r_{\text{eq}}} & -\frac{(1-D)}{L_1} & -\frac{R_B\,(1-D)}{L_1 r_b} \\ 0 & 0 & 0 \\ 0 & -\frac{(1-D)}{L_2} & -\frac{R_B\,(1-D)}{L_2 r_b} \\ 0 & 0 & \frac{R_B}{C_o r_{\text{Co}} r_b} \end{bmatrix} \quad B_d = \begin{bmatrix} 0 \\ \frac{1}{L_1}\left(I_{L1}(R_B + r_{C1}) + V_{C1} + V_D + I_{L2} R_B + \frac{R_B V_{\text{Co}}}{r_{\text{Co}}} + \frac{R_B V_b}{r_b}\right) - \frac{1}{C_1}(I_{L1} + I_{L2}) \\ \frac{1}{L_2}\left(I_{L2}(R_B - r_{C1}) + V_{C1} + V_D + I_{L1} R_B + \frac{R_B V_{\text{Co}}}{r_{\text{Co}}} + \frac{R_B V_b}{r_b}\right) - \frac{R_B}{C_o r_{\text{Co}}}(I_{L1} + I_{L12}) \end{bmatrix}.$$

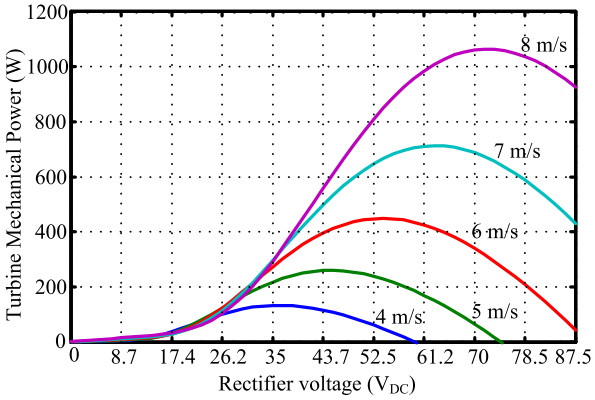

Fig. 3. MPPT converter input voltage and turbine power characteristics.

III. Adaptive MPPT Control Algorithm

At constant wind velocity, wind turbine output power becomes function of power coefficient (2), and at constant pitch angle, power coefficient becomes function of rotor speed as given in (1) and (3). From this discussion, condition for MPP can be obtained as,

$$\frac{dP_m}{d\omega_m} = 0. \tag{12}$$

Applying the chain rule [11], (12) can be written as follows,

$$\frac{dP_m}{d\omega_m} = \frac{dP_m}{dv_{\mathrm{DC}}} \cdot \frac{dv_{\mathrm{DC}}}{d\omega_e} \cdot \frac{d\omega_e}{d\omega_m} = 0. \tag{13}$$

It can be concluded by using (4)–(6),

$$\frac{dP_m}{d\omega_m} = 0 \Leftrightarrow \frac{dP_m}{dv_{\mathrm{DC}}} = 0. \tag{14}$$

Relation between turbine output power and rectifier output voltage is shown in Fig. 3. It is observed that this relation has a corresponding single optimal V_{DC} value for every wind velocity and objective of the proposed algorithm is to search for this optimal operating point $v_{\mathrm{DC_{opt}}}$.

Flowchart of the proposed MPPT algorithm is shown in Fig. 4. Turbine rotor radius *R* and electro motive force (emf) constant K_b (V·s/rad) can be obtained from wind turbine specifications report and open circuit characteristics of WG respectively. Implementation of the algorithm requires a dynamically programmable memory to store system's optimal characteristics in the form of a lookup table and a single-dimensional array. Lookup table holds the optimal relation between wind velocity-optimal dc voltage-maximum output power ($V_w - v_{\mathrm{DC_{opt}}} - P_{\mathrm{DC_{max}}}$) and single-dimensional array keeps the optimal TSR value, λ_{opt}, of the system. Wind velocity column will act as index for the lookup table. Size of the lookup table is limited by the range of the wind velocity and size of the optimal TSR vector is limited to 100 entries. Operating wind velocity range, 3–8 m/s, is written into the index column of the lookup table with the difference of 0.25 m/s between two sequential entries. Initially, all values of $v_{\mathrm{DC_{opt}}}$ and $P_{\mathrm{DC_{max}}}$ in the lookup table are initialized to zero and first entry of optimal TSR vector, $\lambda_{\mathrm{opt}}[1]$, is initialized with a good guess value of 7 [26]. Algorithm reads wind velocity, SEPIC's input voltage and input current for every 10 ms of sampling time. This sampling

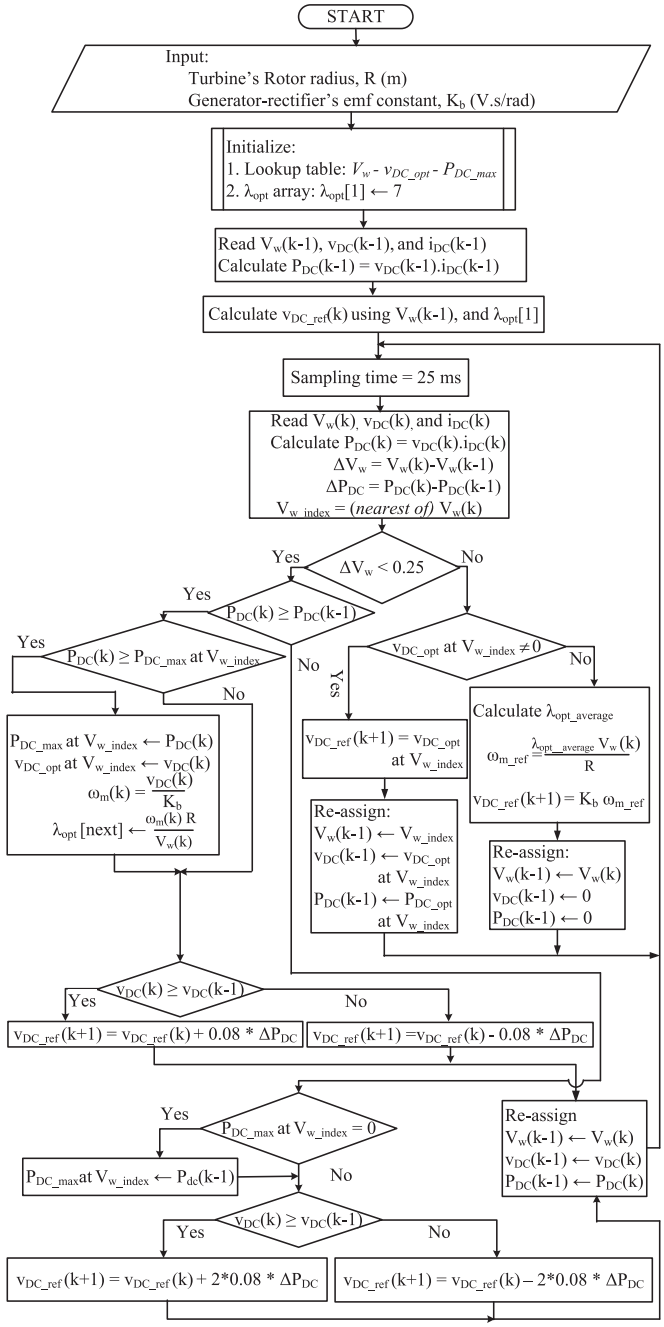

Fig. 4. Adaptive MPPT algorithm flowchart.

frequency of the algorithm is adequately chosen based on the dynamics of the wind turbine. If the difference between two consequent samples of wind velocity is within ± 0.25 m/s, the algorithm treats that the wind is steady wind otherwise turbulent wind.

During steady wind, as described in flowchart, based on the changes in output power with respect to the changes in control variable, algorithm provides reference signal $v_{\mathrm{DC_{ref}}}(k+1)$ by implementing HCS control algorithm. Meanwhile, algorithm performs memory updating computations to optimize the existing data of the lookup table and optimal TSR vector. If the turbine extracts more power compared to previous iteration $P_{\mathrm{DC}}(k) > P_{\mathrm{DC}}(k-1)$, algorithm checks the stored value of $P_{\mathrm{DC_{max}}}$ at the index of the present wind velocity $V_{w_{\mathrm{index}}}$ in

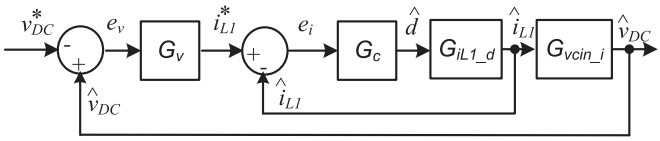

Fig. 5. Double loop current-mode control structure.

TABLE I
SEPIC CONVERTER PARAMETERS

Parameter	Value
Thevenin eq. resistance, $r_{\rm eq}$ (mΩ)	2.2
Input capacitance, $C_{\rm in}$ (μF)	30
ESR of input capacitor $r_{C\,\rm in}$ (mΩ)	1.0
Input inductor, L_1 (mH)	8.7
ESR of input inductor, $r_{L\,1}$ (mΩ)	1.0
Coupling capacitor, C_1 (μF)	90
ESR of coupling capacitor, $r_{C\,1}$ (mΩ)	3.0
Output inductor, L_2 (mH)	8.7
ESR of output inductor, $r_{L\,2}$ (mΩ)	1.0
Output capacitor, C_o (μF)	500
ESR of output capacitor, $r_{\rm Co}$ (mΩ)	3.0
Battery internal resistor, r_b (mΩ)	34.2

lookup table and updates the memory if $P_{\rm DC}(k) > P_{\rm DC_{max}}$ at $V_{w_{\rm index}}$ as depicted in flowchart. After updating the lookup table, updated value for TSR is calculated and is filled at the next entry location of the optimal TSR vector as follows,

$$\lambda_{\rm opt}\,[\text{next}] \leftarrow \frac{\omega_m(k)R}{V_w(k)}. \tag{15}$$

Whenever wind turbine operates with better optimal performance than the stored operating point at a given wind velocity, algorithm modifies the programmable memory. These continuous modifications of the memory towards the optimal operating points enable the algorithm to acquire optimal characteristics of the given WECS. This adaptivity feature of the algorithm makes it suitable to apply on wide range of WECSs.

During turbulent wind conditions, algorithm provides reference signal by implementing either PSF or TSR algorithmic computations. Algorithm searches the lookup table for $v_{\rm DC_{opt}}$ at $V_w(k)$ index. If the entry of $v_{\rm DC_{opt}}$ at $v_{w_{\rm index}}$ is nonzero, PSF control algorithm will be implemented by giving this entry as reference value $v_{\rm DC_{ref}}(k+1)$ for the next iteration. If the value of $v_{\rm DC_{opt}}$ at $v_{w_{\rm index}}$ is zero, algorithm implements TSR control. Average of the optimal TSR vector $\lambda_{\text{opt-average}}$ is considered as system $\lambda_{\rm opt}$ and reference voltage $v_{\rm DC_{ref}}(k+1)$ is calculated by using K_b as described in flowchart. Implementation of the PSF and TSR control computations by using programmable memory feature allows the system to immediately jump to the optimal operating point, thereby bypassing the time-consuming searching procedure. Once all the entries of $v_{\rm DC_{opt}}$ in lookup table are filled with nonzero values, then implementation of TSR algorithm will be discarded. Application of stored information facilitates the proposed algorithm to improve the dynamic response of the system. Moreover, self learning of system specific characteristics makes this algorithm adaptive in nature. The adaptability of the algorithm allows the system to extract as much available wind

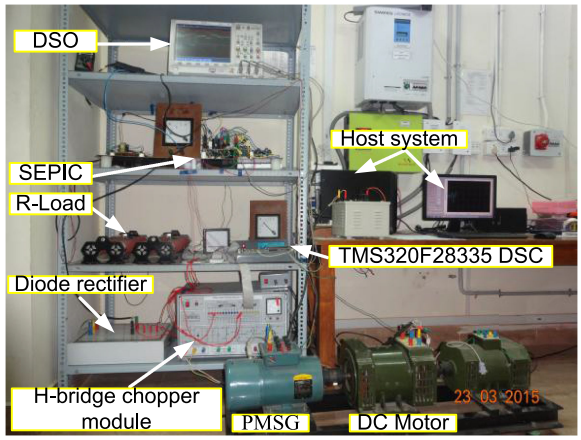

Fig. 6. Experimental setup.

power as possible under turbulent wind conditions.

$$G_{i_{L\,1}d}(s) = \frac{\hat{i}_{L\,1}(s)}{\hat{d}(s)}|_{\hat{u}(s)=0} =$$

$$\frac{1.3802e05\,(s+1.515e05)\,(s+249.6)\,(s^2+116.7s+7.937e06)}{(s+1.515e05)\,(s^2+209.2s+1.43e06)\,(s^2+5s+7.937e06)} \tag{16}$$

$$G_{v_{C\,\rm in}d}(s) = \frac{\hat{v}_{C\,\rm in}(s)}{\hat{d}(s)}|_{\hat{u}(s)=0}$$

$$= \frac{-4.1823e07\,(s+249.6)\,(s^2+116.7s+7.937e06)}{(s+1.515e05)\,(s^2+209.2s+1.43e06)\,(s^2+5s+7.937e06)} \tag{17}$$

$$G_{v_{C\,\rm in}i_{L\,1}}(s) = \frac{\hat{v}_{C\,\rm in}(s)}{\hat{i}_{L\,1}(s)}|_{\hat{u}(s)=0} = \frac{G_{v_{C\,\rm in}d}(s)}{G_{i_{L\,1}d}(s)}|_{\hat{u}(s)=0}$$

$$= -\frac{R_{\rm eq}r_{\rm eq}}{(R_{\rm eq}+C_{\rm in}r_{C\,\rm in}r_{\rm eq}s)} = -\frac{0.002}{(4.4e-6s+1)}. \tag{18}$$

IV. COMPENSATOR DESIGN

A. SEPIC Based Plant's Transfer Functions

In this work, dual-loop current mode control, as shown in Fig. 5 is implemented for faster dynamic response and to avoid the right half plane zero issue in continuous conduction mode (CCM) operation of the SEPIC converter. Designed parameters for CCM operation of SEPIC converter are given in Table I. The required transfer functions for the controller design are derived from the small-signal state-space model of the plant given in (11) by applying Laplace transform and are given in (16)–(18).

B. Digital Controller Design

Proportional gain along with a dominant pole with zero compensation [27] controllers are tuned for faster inner current loop (phase margin $= 75.6^\circ$ at gain cross-over frequency $= 3.28 \times 10^4$ rad/s) and relatively slower outer voltage loop (phase margin $= 56.3^\circ$ at gain cross-over frequency $= 3.08 \times 10^4$ rad/s). Digital redesign approach [28] is used in this work for the development of the compensators. While transforming into discrete-time domain by using matched pole-zero method [29], sampling

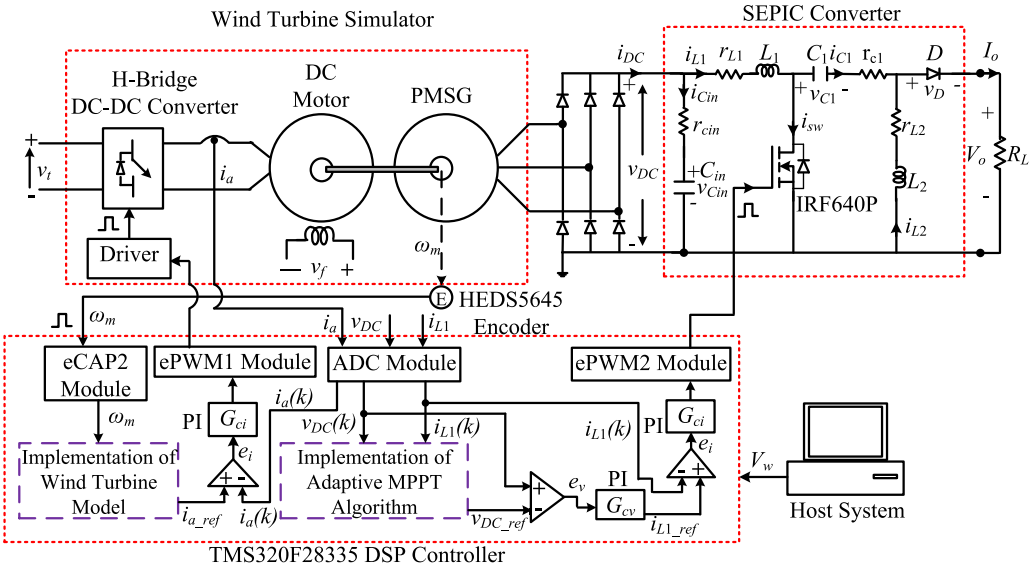

Fig. 7. Experimental setup block schematic.

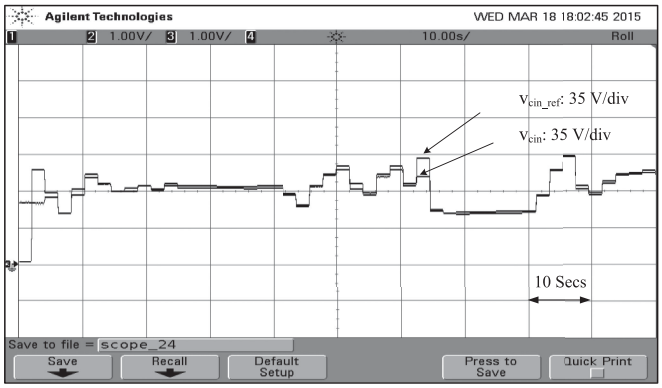

Fig. 8. SEPIC's reference signal tracking response.

frequency is set at 50 kHz and the designed compensators are as follows,

$$G_c(z) = \frac{3.095z - 2.619}{z - 1}$$
$$G_v(z) = \frac{1.259z - 1.133}{z - 1}. \quad (19)$$

V. Experimental Results

An experimental setup shown in Fig. 6, has been developed for the performance evaluation of the proposed MPPT control algorithm in extracting maximum power by a given WECS. Schematic of this test rig is shown in Fig. 7.

SEPIC dc–dc converter's response in reference signal tracking with double loop current mode controller has been verified and is shown in Fig. 8. The observed performance ensures that the tracking behavior of the converter is satisfactory even at wide variations in reference signal.

A. Wind Turbine Simulator

TMS320F28335 DSC based variable speed DC motor drive system with torque control was developed to emulate the

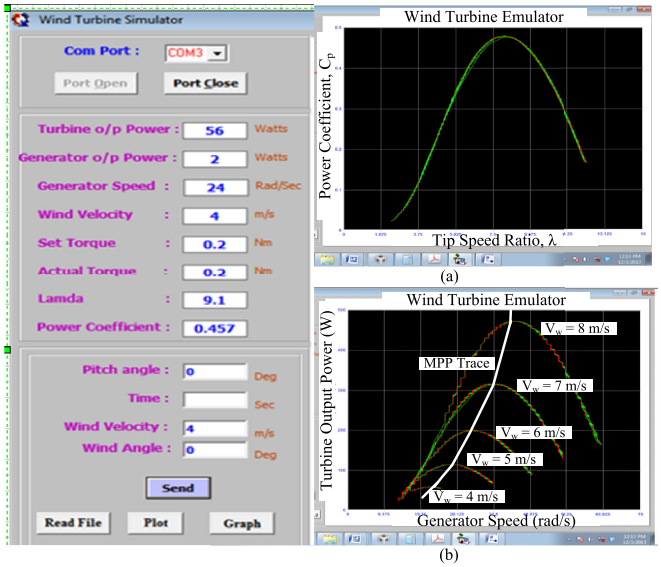

Fig. 9. Wind turbine emulation. (a) Variation of C_p versus λ. (b) Variation of P_m versus ω_m .

characteristics of real wind turbine. This hardware simulator can be used for understanding the behavioral characteristics of WECS and to evaluate the performance of newly proposed MPPT control algorithms. In host system, a graphical user interface environment is designed to display the relations between various parameters of the emulated wind turbine. For a given wind velocity, variations in C_p as a function of TSR are shown in Fig. 9(a). It can be observed from Fig. 9(a) that maximum power coefficient $C_{p_{max}}$ of emulated WECS is 4.789 at optimal TSR λ_{opt} of 8.1. Fig. 9(b) shows emulated wind turbine mechanical power as a function of rotor speed at various wind speeds.

B. Performance Evaluation of Proposed MPPT Algorithm

After running the system with proposed MPPT algorithm for the duration of 5000 s, it is observed that average value

TABLE II
LOOKUP TABLE OF MAXIMUM POWER CHARACTERISTICS

V_w	3.25	3.5	3.75	4.0	4.25	4.5	4.75	5.0	5.25	5.5	5.75	6.0	6.25	6.5	6.75	7.0
$v_{\mathrm{DC_{opt}}}$	21.3	46.7	47.1	48.8	53.6	56.6	59.1	82.11	66.98	70.94	74.14	82.36	85.84	86.81	91.28	94.6
$P_{\mathrm{DC_{max}}}$	12.2	30.1	30.3	33.2	35.1	45.1	54.8	76.1	81.1	95.6	109.2	143.1	162.7	178.3	200.6	222.5

of the optimal TSR vector $\lambda_{\text{opt-average}}$ is 7.91 and data stored in lookup table is presented in Table II. In this section, behavior of the WECS with proposed MPPT algorithm is analyzed by using two stages of evaluations. In first stage, effectiveness of the proposed MPPT algorithm is evaluated by observing the system performance in extracting maximum power under sudden and gradually varying wind conditions. In second stage of evaluation, a comparative study has been done between system performance with conventional HCS algorithm and proposed MPPT algorithm against turbulent wind conditions.

1) System Performance With Proposed MPPT Algorithm: Fig. 10 shows performance of the WECS with proposed MPPT algorithm under sudden and gradual varying wind conditions. In Fig. 10(a), at time t_1, when system experiences a sudden variation in wind velocity from 4.5 to 6.5 m/s, algorithm executes turbulent wind condition related computations and searches the lookup table for $v_{\mathrm{DC_{opt}}}$ at the index wind velocity of 6.5 m/s. Since the data at $v_{\mathrm{DC_{opt}}}$ is 86.81, algorithm implements PSF feature and provides reference signal immediately to the controller without any random search process. During next sampling time, $(t_1 + 25\,\text{ms})$, since the wind velocity remains at 6.5 m/s, algorithm implements HCS feature and updates the programmable memory's $P_{\mathrm{DC_{max}}}$ and $v_{\mathrm{DC_{opt}}}$ if it observes that $(t_1 + 25\,\text{ms}) > P_{\mathrm{DC}}(t_1)$. At t_2, when wind velocity reduces to 5 m/s, algorithm retrieves optimal characteristics from the lookup table and generates reference signal $v_{\mathrm{DC_{opt}}}$ as 82.11 V by implementing PSF feature of the algorithm under turbulent wind condition related computations. From t_2 to t_3, performance of the WECS is observed during gradual variations in wind velocity from 4.75 to 7 m/s and then from 7 to 4.75 m/s. Variations in power coefficient between t_1 and t_3 are nearly 4.7 and this ensures the optimal performance of the system throughout the duration under turbulent and gradual wind varying conditions. To ensure the system's optimal performance, similar wind velocity conditions are applied to the system from t_3 to t_6, and it can be observed that system operation is always near to MPP. Variations in C_p w.r.t. TSR and turbine power P_m w.r.t. turbine speed ω_m are shown in Fig. 10(b) and (c) respectively. These results confirm the optimal performance of the WECS throughout the fast as well as gradually varying wind velocity conditions. Moreover, proposed algorithm's continuous modifications in programmable memory during its implementation, make the optimal tracking performance of the system more effective and efficient.

2) Comparative Study of System Performance With HCS Algorithm and Proposed MPPT Algorithm: System performance with HCS algorithm and proposed MPPT algorithm under fluctuating wind conditions are compared in this section. HCS

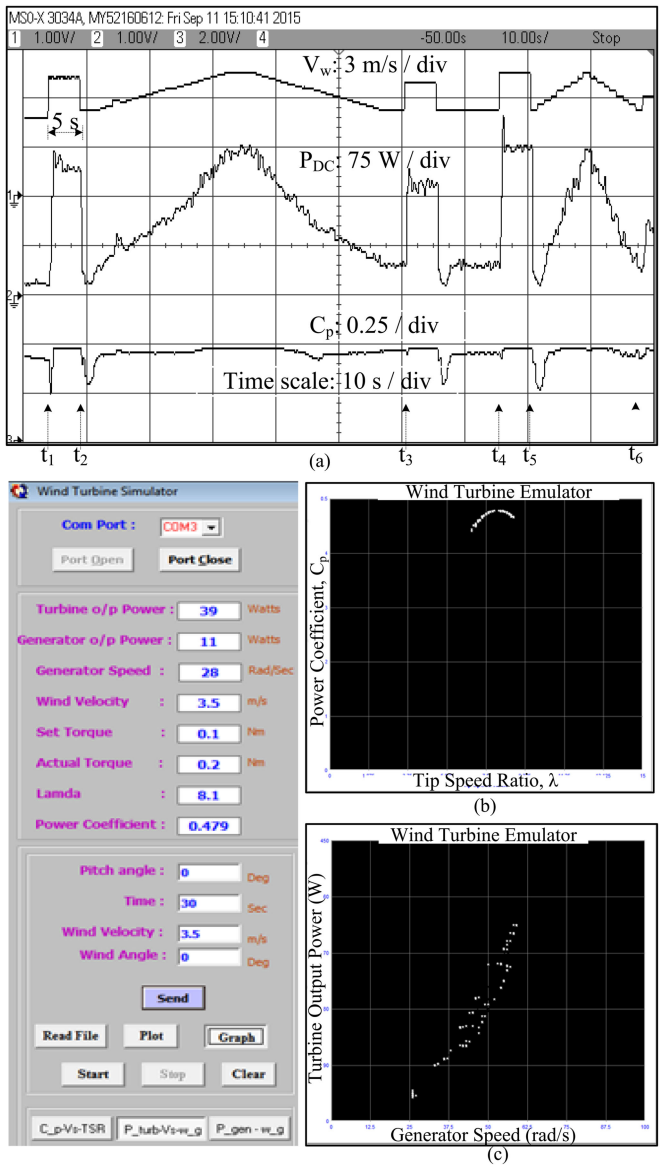

Fig. 10. Performance of WECS with proposed MPPT algorithm. (a) Dynamic response under varying wind conditions. (b) Power coefficient variations. (c) Extracted output power.

algorithm provides reference signal by using

$$v_{\mathrm{DC_{ref}}}(k+1) = v_{\mathrm{DC_{ref}}}(k) + \eta \cdot (P_{\mathrm{DC}}(k) - P_{\mathrm{DC}}(k-1)) \tag{20}$$

where η is incremental step factor. System response with HCS algorithm is shown in Fig. 11(a) and (b). Fig. 11(c) and (d) show the performance of the system with proposed MPPT algorithm.

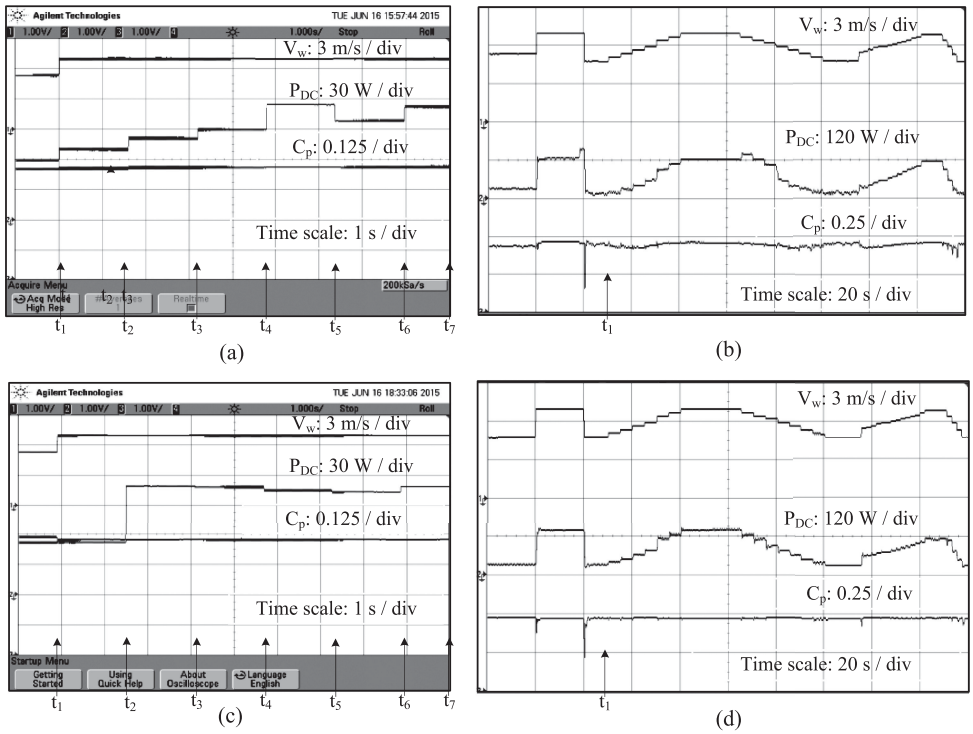

Fig. 11. Performance evaluation of proposed MPPT algorithm. (a), (b) Performance with HCS algorithm. (c), (d) Performance with proposed algorithm.

In Fig. 11(a), at instant t_1, when wind velocity changes suddenly from 5 to 6.5 m/s, HCS algorithm needs four adjustment cycles before reaching to the optimal operating point. Whereas, proposed algorithm provides reference signal $v_{\mathrm{DC_{opt}}}(k+1) = 86.81$ V by using lookup table data and it places the system promptly at MPP without any arbitrary variations as shown in Fig. 11(c). Time lapse between t_n and t_{n+1} is 1.5 s and is given to allow the wind turbine emulator to respond for the changes in wind velocity and load. Energy harvested by the system is calculated as per

$$W = \sum\nolimits_i (P_{\mathrm{DC}} \text{ during } \mathrm{t_i} \text{ and } \mathrm{t_{i+1}}) \cdot (\mathrm{t_{i+1}} - \mathrm{t_i}). \quad (21)$$

According to (21), proposed algorithm extracts 2.0625 Wh, whereas HCS algorithm extracts 1.3875 Wh against similar wind profile from t_1 to t_7. System response with HCS algorithm against gradual variations in wind velocity is shown in Fig. 11(b). During continuous variations in wind velocity from instant t_1, system tries to track the MPP. However, fluctuations in wind velocity cause the searching process to start from an arbitrary point every time and this makes the tracking performance inefficient. This is indicated by the deviations in C_p from its optimal point as shown in Fig. 11(b). Whereas proposed algorithm makes the system to track MPP immediately without any intermediate random search operations as shown in Fig. 11(d). By observing the variations in C_p, it can be concluded that WECS with proposed algorithm harvests more energy than with HCS algorithm.

VI. Conclusion

In this paper, an adaptive MPPT control algorithm has been proposed for the fast tracking of MPP under turbulent wind conditions for small-scale WECSs. System behavior with proposed algorithm under fast changing wind conditions has been observed and it is evident that the proposed control algorithm can put the system at optimal operating point promptly against random variations in the wind velocity. System performance with proposed algorithm is compared with the HCS algorithm and experimental results proved that WECS with proposed algorithm harvests more energy than with HCS algorithm. The proposed algorithm provides the following advantages: 1) improved dynamic response of the system; 2) prerequisite of system's optimal characteristics data is not required and hence the algorithm is adaptive; and 3) algorithm's continuous modifications on programmable memory towards optimal characteristics of the system, eliminate the possibility of system's performance degradation due to parameters variations. To extract maximum power from the wide range of wind conditions, SEPIC converter is used for the implementation of proposed MPPT algorithm. Since small-scale WECSs are main resources for DERs in microgrid systems, the proposed algorithm is very much applicable for microgrid systems.

References

[1] D. S. Zinger and E. Muljadi, "Annualized wind energy improvement using variable speeds," *IEEE Trans. Ind. Appl.*, vol. 33, no. 6, pp. 1444–1447, Nov./Dec. 1997.

[2] A. Miller, E. Muljadi, and D. Zinger, "A variable speed wind turbine power control," *IEEE Trans. Energy Convers.*, vol. 12, no. 2, pp. 181–186, Jun. 1997.

[3] R. Chedid, F. Mrad, and M. Basma, "Intelligent control of a class of wind energy conversion systems," *IEEE Trans. Energy Convers.*, vol. 14, no. 4, pp. 1597–1604, Dec. 1999.

[4] H. Li, K. Shi, and P. McLaren, "Neural-network-based sensorless maximum wind energy capture with compensated power coefficient," *IEEE Trans. Ind. Appl.*, vol. 41, no. 6, pp. 1548–1556, Nov./Dec. 2005.

[5] A. S. Satpathy, N. Kishore, D. Kastha, and N. Sahoo, "Control scheme for a stand-alone wind energy conversion system," *IEEE Trans. Energy Convers.*, vol. 29, no. 2, pp. 418–425, Jun. 2014.
[6] S. Morimoto, H. Nakayama, M. Sanada, and Y. Takeda, "Sensorless output maximization control for variable-speed wind generation system using ipmsg," in *Proc. IEEE 38th Ind. Appl. Annu. Meeting Conf. Rec.*, 2003, vol. 3, pp. 1464–1471.
[7] R. M. Hilloowala and A. M. Sharaf, "A rule-based fuzzy logic controller for a pwm inverter in a stand alone wind energy conversion scheme," in *Proc. IEEE Ind. Appl. Soc. Annu. Meeting Conf. Rec.*, 1993, pp. 2066–2073.
[8] V. Galdi, A. Piccolo, and P. Siano, "Designing an adaptive fuzzy controller for maximum wind energy extraction," *IEEE Trans. Energy Convers.*, vol. 23, no. 2, pp. 559–569, Jun. 2008.
[9] A. Raju, B. Fernandes, and K. Chatterjee, "A upf power conditioner with maximum power point tracker for grid connected variable speed wind energy conversion system," in *Proc. IEEE 1st Int. Conf. Power Electron. Syst. Appl.*, 2004, pp. 107–112.
[10] M. Chinchilla, S. Arnaltes, and J. C. Burgos, "Control of permanent-magnet generators applied to variable-speed wind-energy systems connected to the grid," *IEEE Trans. Energy Convers.*, vol. 21, no. 1, pp. 130–135, Mar. 2006.
[11] E. Koutroulis and K. Kalaitzakis, "Design of a maximum power tracking system for wind-energy-conversion applications," *IEEE Trans. Ind. Electron.*, vol. 53, no. 2, pp. 486–494, Apr. 2006.
[12] S. M. R. Kazmi, H. Goto, H.-J. Guo, and O. Ichinokura, "A novel algorithm for fast and efficient speed-sensorless maximum power point tracking in wind energy conversion systems," *IEEE Trans. Ind. Electron.*, vol. 58, no. 1, pp. 29–36, Jan. 2011.
[13] Q. Wang and L. Chang, "An intelligent maximum power extraction algorithm for inverter-based variable speed wind turbine systems," *IEEE Trans. Power Electron.*, vol. 19, no. 5, pp. 1242–1249, Sep. 2004.
[14] J. Hui and A. Bakhshai, "A new adaptive control algorithm for maximum power point tracking for wind energy conversion systems," in *Proc. IEEE Power Electron. Spec. Conf.*, 2008, pp. 4003–4007.
[15] M. Zadeh, A. Hajimiragha, M. Adamiak, A. Palizban, and S. Allan, "Design and implementation of a microgrid controller," in *Proc. 64th Annu. Conf. Protective Relay Eng. Conf.*, 2011, pp. 137–145.
[16] J. Carroll, A. McDonald, and D. McMillan, "Reliability comparison of wind turbines with dfig and pmg drive trains," *IEEE Trans. Energy Convers.*, vol. 30, no. 2, pp. 663–670, Jun. 2015.
[17] W. Wu, V. Ramsden, T. Crawford, and G. Hill, "A low speed, high-torque, direct-drive permanent magnet generator for wind turbines," in *Proc. IEEE Ind. Appl. Conf. Rec.*, 2000, vol. 1, pp. 147–154.
[18] Z. M. Dalala, Z. U. Zahid, W. Yu, Y. Cho, and J.-S. Lai, "Design and analysis of an mppt technique for small-scale wind energy conversion systems," *IEEE Trans. Energy Convers.*, vol. 28, no. 3, pp. 756–767, Sep. 2013.
[19] C.-T. Pan and Y.-L. Juan, "A novel sensorless mppt controller for a high-efficiency microscale wind power generation system," *IEEE Trans. Energy Convers.*, vol. 25, no. 1, pp. 207–216, Mar. 2010.
[20] G. L. Johnson, *Wind Energy Systems*. Englewood Cliffs, NJ, USA: Prentice-Hall, 2006.
[21] Z. Salameh *et al.*,"Modeling and simulation of a wind turbine-generator system," in *Proc. IEEE Power Energy Soc. Gen. Meeting*, 2011, pp. 1–7.
[22] N. Mohan and T. M. Undeland, *Power Electronics: Converters, Applications, and Design*. Hoboken, NJ, USA: Wiley, 2007.
[23] S. Chiang, H.-J. Shieh, and M.-C. Chen, "Modeling and control of pv charger system with sepic converter," *IEEE Trans. Ind. Electron.*, vol. 56, no. 11, pp. 4344–4353, Nov. 2009.
[24] H. S.-H. Chung, K. Tse, S. R. Hui, C. Mok, and M. Ho, "A novel maximum power point tracking technique for solar panels using a sepic or cuk converter," *IEEE Trans. Power Electron.*, vol. 18, no. 3, pp. 717–724, May 2003.
[25] R. W. Erickson and D. Maksimovic, *Fundamentals of Power Electronics*. New York, NY, USA: Springer, 2007.
[26] N. Cetin, M. Yurdusev, R. Ata, and A. Özdemir, "Assessment of optimum tip speed ratio of wind turbines," *Math. Comput. Appl.*, vol. 10, no. 1, pp. 147–154, 2005.
[27] C.-C. Hang, Q. Bi *et al.*, "A frequency domain controller design method," *Chem. Eng. Res. Des.*, vol. 75, no. 1, pp. 64–72, 1997.
[28] A. Emadi, A. Khaligh, Z. Nie, and Y. J. Lee, *Integrated Power Electronic Converters and Digital Control*. Boca Raton, FL, USA: CRC Press, 2009.
[29] G. F. Franklin, J. D. Powell, and M. L. Workman, *Digital Control of Dynamic Systems*, vol. 3. Menlo Park, CA, USA: Addison-Wesley, 1998.

Jakeer Hussain (S'09) received the Bachelor's degree in electrical engineering from the National Institute of Technology, Warangal, India, in 1999, and the Master of Engineering degree in Industrial Drives and Control from the Osmania University College of Engineering, Hyderabad, India, in 2003. He is currently working toward the Ph.D. degree in electrical engineering at the Indian Institute of Technology Madras, Chennai, India. His research interests include power electronic converters design for renewable energy applications, development of nonlinear controllers, and coordination and control of renewable energy sources.

Mahesh K. Mishra (S'00–M'02–SM'10) received the B.Tech. degree in electrical engineering from the College of Technology, Pantnagar, India, in 1991; the M.E. degree in electrical engineering from the University of Roorkee, Roorkee, India, in 1993; and the Ph.D. degree in electrical engineering from the Indian Institute of Technology, Kanpur, India, in 2002.

He has teaching and research experience of about 23 years. For about ten years, he was with the Electrical Engineering Department, Visvesvaraya National Institute of Technology, Nagpur, India. He is currently a Professor with the Electrical Engineering Department, Indian Institute of Technology Madras, Chennai. His research interests include the areas of power distribution systems, power electronics, microgrids, and renewable energy systems.

Dr. Mahesh is a Life Member of the Indian Society of Technical Education.